PCCP

PAPER

Cite this: *Phys. Chem. Chem. Phys.*, 2018, **20**, 26734

Direct solid state NMR observation of the ^{105}Pd nucleus in inorganic compounds and palladium metal systems†‡

Thomas J. N. Hooper,[a] Thomas A. Partridge,[a] Gregory J. Rees,[a] Dean S. Keeble,[b] Nigel A. Powell,[c] Mark E. Smith,[d] Iryna P. Mikheenko,[e] Lynne E. Macaskie,[e] Peter T. Bishop[c] and John V. Hanna*[a]

The ability to clearly relate local structure to function is desirable for many catalytically relevant Pd-containing systems. This report represents the first direct ^{105}Pd solid state NMR measurements of diamagnetic inorganic ($K_2Pd(IV)Cl_6$, $(NH_4)_2Pd(IV)Cl_6$ and $K_2Pd(IV)Br_6$) complexes, and micron- and nano-sized Pd metal particles at room temperature, thereby introducing effective ^{105}Pd chemical shift and Knight shift ranges in the solid state. The very large ^{105}Pd quadrupole moment (Q) makes the quadrupole parameters (C_Q, η_Q) extremely sensitive to small structural distortions. Despite the well-defined high symmetry octahedral positions describing the immediate Pd coordination environment, ^{105}Pd NMR measurements can detect longer range disorder and anisotropic motion in the interstitial positions. The approach adopted here combines high resolution X-ray pair distribution function (PDF) analyses with ^{105}Pd, ^{39}K and ^{35}Cl MAS NMR, and shows solid state NMR to be a very sensitive probe of short range structural perturbations. Solid state ^{105}Pd NMR observations of ~44–149 μm Pd sponge, ~20–150 nm Pd black nanoparticles, highly monodisperse 16 ± 3 nm PVP-stabilised Pd nanoparticles, and highly polydisperse ~2–1100 nm biomineralized Pd nanoparticles (bio-Pd) on pyrolysed amorphous carbon detect physical differences between these systems based on relative bulk:surface ratios and monodispersity/size homogeneity. This introduces the possibility of utilizing solid state NMR to help elucidate the structure–function properties of commercial Pd-based catalyst systems.

Received 24th April 2018,
Accepted 31st August 2018

DOI: 10.1039/c8cp02594k

rsc.li/pccp

Introduction

The accessible oxidation states, flexibility and relatively lower cost in comparison to other precious metals makes Pd a viable option in many industrial, technological and catalytic processes.[1–3] The most prominent uses of Pd involve its application to hydrogenation reactions of fatty acids and the cracking of petrochemical systems, dental applications, hydrogen fuel cells, and important automotive catalytic applications which realise NO_x/SO_x reduction and the abatement of other greenhouse gas emissions.[1] When alloyed with Pt, it is key component of car exhaust catalytic converters due to its resistance to both oxidation and high temperature corrosion.

The excessive functional demands on modern materials require highly accurate refinements of their proposed crystal structures. Most catalytic applications of Pd involve the use of organometallic Pd systems, or the deployment of pure or alloyed Pd metal nanoparticles (and sometimes sub-micron/micron particles) on various substrates and which often assume layered arrangements. This renders the characterisation by conventional techniques such as X-ray diffraction (XRD) somewhat problematic, and these systems often lack the effective long-range order that enables these measurements. The short-range, element specific nature of techniques such as solid state NMR provide a useful alternative that can readily probe structural aspects of materials that lack long-range order. It can be an excellent probe for characterising disordered systems, and it exhibits great complementarity with other techniques such as diffraction and vibrational spectroscopies.

No thorough NMR investigation of the ^{105}Pd nucleus in diamagnetic materials has ever been undertaken and the field of ^{105}Pd solid state NMR is undeveloped and unexplored.

---

[a] *Department of Physics, University of Warwick, Coventry, CV4 7AL, UK. E-mail: j.v.hanna@warwick.ac.uk*
[b] *Diamond Light Source, Harwell Science and Innovation Campus, Didcot, OX11 0DE, UK*
[c] *Johnson Matthey Technology Centre, Reading, RG4 9NH, UK*
[d] *University of Lancaster, Lancaster, LA1 4YW, UK*
[e] *School of Biosciences, University of Birmingham, Birmingham, B15 2TT, UK*

† The experimental data for this study are provided as a supporting dataset from WRAP, the Warwick Research Archive Portal at http://wrap.warwick.ac.uk/108012.

‡ Electronic supplementary information (ESI) available. See DOI: 10.1039/c8cp02594k

The dearth of ^{105}Pd solid state NMR studies has largely been a consequence of the extremely large quadrupole moment (Q = 66 fm^2, I = 5/2),[4] low gyromagnetic ratio ($\gamma = -1.23 \times 10^7$ rad s^{-1} T^{-1}), and modest natural abundance of the ^{105}Pd nucleus at 22%.[5] To date, these combined factors have hampered ^{105}Pd measurements to the point where only very high-symmetry (cubic) metallic palladium environments, mostly at low temperatures, have been reported.[6–9] However, the large quadrupole moment makes this nucleus extremely sensitive to small structural variations at the Pd position. This phenomenon allows the detection of extremely small structural variations, and when coupled with techniques such as X-ray pair distribution function (PDF) analyses, an unprecedented level of structural accuracy can be achieved. This study is the first report of ^{105}Pd solid state NMR of diamagnetic materials, and this is demonstrated on Pd(IV)-hexahalo complexes with supposedly high octahedral point symmetry.

The ^{105}Pd static NMR technique is then adopted to study Pd metal particles of very different size and morphology. Micron-sized Pd metal sponge, nano-sized Pd metal black and nano-sized poly(*N*-vinyl-2-pyrrolidone) (PVP) stabilised Pd nanoparticles are all relevant functional materials in industrial processes such as hydrogen storage and catalysis of fine chemical synthesis.[10–12] The ^{105}Pd Knight shift is very sensitive to physical differences and it can highlight some important aspects of the catalytic interface and the different electronic properties of the system.

Results and discussion

A first step in the development of a methodology for studying an NMR-active nucleus is to determine an appropriate isotropic chemical shift reference to standardize all ^{105}Pd chemical shift measurements. The IUPAC recommended reference K_2PdCl_6 (in D_2O) is of limited use as the low solubility of this complex in aqueous solutions and the broad ^{105}Pd linewidth limit its general applicability. Fedotov *et al.*[13] previously observed the ^{105}Pd solution NMR resonance of $H_2Pd(IV)Cl_6$ (octahedral Pd point symmetry), however their synthetic route facilitates the fast reduction to $H_2Pd(II)Cl_4$ (planar Pd point symmetry), an observation supported by many industrial processes and extractions at low pH.[14] This species yields a very broad ^{105}Pd resonance in solution which offers very limited resolution and accuracy as a chemical shift standard. This study proposes a 0.33 M solution of $H_2PdCl_{6(aq)}$ in *aqua regia* (conc. $HCl_{(aq)}$: conc. $HNO_{3(aq)}$ = 3 : 1) as a chemical shift standard, as the higher symmetry Pd(IV) species is maintained under these conditions; this synthetic route is described in the Experimental section. As demonstrated in the Supplementary Section (SI1, ESI‡), the ^{105}Pd chemical shift from H_2PdCl_6 exhibits a minor concentration dependence with the shift variation in *aqua regia* decreasing at low concentrations of ≤0.15 M.

Furthermore, the proximity to a convenient external solid state reference $KCl_{(s)}$ is also proposed to be very effective, thus eliminating the repetitive handling of *aqua regia* solutions in solid state NMR probes. The utility of both $H_2Pd(IV)Cl_{6(aq)}$ and $KCl_{(s)}$ referencing approaches is shown in Fig. 1(a) which demonstrates the consistency of these shifts across all B_0 field strengths.

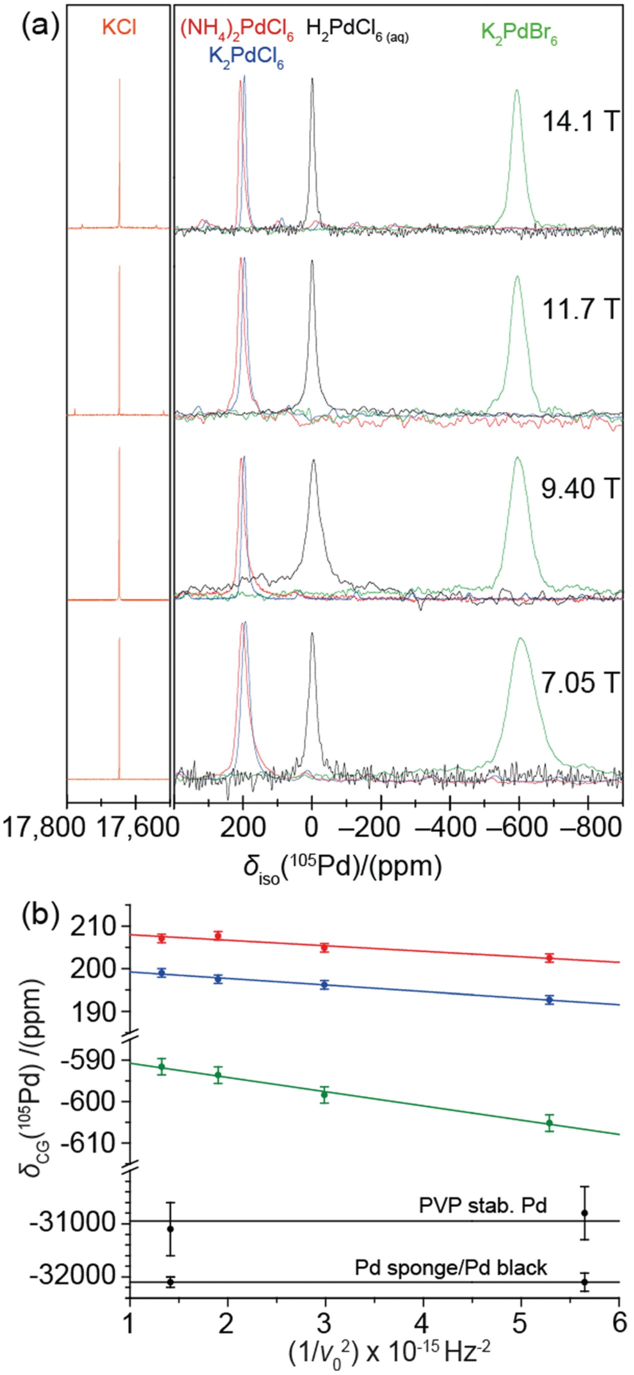

Fig. 1 (a) The ^{105}Pd NMR spectra of the primary reference $H_2PdCl_{6(aq)}$ (black) at δ_{iso} = 0.0 ppm, the secondary reference $KCl_{(s)}$ (orange) and three octahedral palladium compounds: $(NH_4)_2PdCl_{6(s)}$ (red), $K_2PdCl_{6(s)}$ (blue) and $K_2PdBr_{6(s)}$ (green). The spectra were acquired at 14.1 T (υ_0 = 27.49 MHz), 11.7 T (υ_0 = 22.93 MHz), 9.40 T (υ_0 = 18.30 MHz) and 7.05 T (υ_0 = 13.75 MHz) with an MAS frequency of υ_0 = 3 kHz for the solid samples. (b) The ^{105}Pd centre-of-gravity shifts (δ_{CG}) from $(NH_4)_2PdCl_6$ (red), K_2PdCl_6 (blue), K_2PdBr_6 (green), Pd sponge/black and PVP stabilised Pd nanoparticles (black) against the inverse square of the Larmor frequency (υ_0) at 14.1 T, 11.7 T, 9.40 T and 7.05 T.

The cubic point symmetry of K in the KCl lattice rigorously restricts the ^{39}K quadrupolar coupling constant (C_Q)[15,16] to be zero thus creating a field independent reference in the solid state; this has been verified against $KCl_{(aq)}$.[17] The ^{39}K nucleus is conveniently close to ^{105}Pd in frequency with a gyromagnetic ratio of -1.23×10^7 rad s^{-1} T^{-1}, thereby requiring only minimal retuning of the NMR probe upon switching observation. The $H_2PdCl_{6(aq)}$ solution reference shift was set to 0.0 ppm and the ^{39}K resonance of $KCl_{(s)}$ was recorded at a shift position of 17 647 ppm at four fields (14.1 T, 11.7 T, 9.40 T and 7.05 T). This field independence of the ^{105}Pd chemical shift confirms that the H_2PdCl_6 species does not have a measurable ^{105}Pd quadrupolar coupling constant C_Q, as observed in some solutions containing species which possess large quadrupole moments Q.[18]

Solid state ^{105}Pd NMR and X-ray PDF analyses have been utilised to investigate three model diamagnetic inorganic Pd(IV) complexes to establish the observable chemical shift range, and to investigate the small reduction in symmetry that occurs in the notionally high-symmetry octahedral Pd coordination. According to previously reported powder XRD studies, all three systems are characterised by a face centred cubic (FCC) structure (space group $Fm\bar{3}m$) in which the Pd(IV) centre occupies a rigidly octahedral environment.[19] Despite the quadrupolar nature of the $I = 5/2$ ^{105}Pd nucleus there should be no electric field gradient (EFG) at these Pd(IV) positions, and hence no measurable 2nd order quadrupolar contribution augmenting the isotropic chemical shift (δ_{iso}). A multi-field MAS NMR study of the solid $(NH_4)_2Pd(IV)Cl_6$, $K_2Pd(IV)Cl_6$ and $K_2Pd(IV)Br_6$ systems is also shown in Fig. 1(a). In contrast to the chemical shift references proposed above, the ^{105}Pd MAS NMR data from the three complexes exhibits distinct variable field behaviour as clearly shown in Fig. 1(b). For any quadrupolar nucleus the apparent/measurable chemical shift (δ_{cg}) is comprised of both field independent isotropic chemical shift (δ_{iso}) and field dependent second-order quadrupolar shift ($\delta^{(2)}_{Q,iso}$) components:[20–23]

$$\delta_{cg} = \delta_{iso} + \delta^{(2)}_{Q,iso}(I,m) \qquad (1)$$

where

$$\delta^{(2)}_{Q,iso}(I,m) = \left(3C_Q{}^2/(40\nu_o{}^2I^2(2I-1)^2)\right)$$
$$[I(I+1) - 9m(m-1) - 3](1 + \eta_Q{}^2/3) \qquad (2)$$

When considering the central transition (*i.e.* $m = \frac{1}{2}$) for a spin $I = 5/2$ nucleus such as ^{105}Pd, eqn (2) reduces to:

$$\delta^{(2)}_{Q,iso} = \left(6C_Q{}^2/(1000\nu_o{}^2)(1 + \eta_Q{}^2/3)\right) \qquad (3)$$

From the variable field data of Fig. 1(a) further analysis enables δ_{iso} to be determined graphically from the y-intercept of this behaviour, and the quadrupole product (P_Q) defined as:

$$P_Q = C_Q\sqrt{(1 + \eta_Q{}^2/3)} \qquad (4)$$

can be determined from the slope. This treatment of the data shown in Fig. 1(b) yields isotropic chemical shifts δ_{iso} of 209 ± 2 ppm, 201 ± 2 ppm and −585 ± 3 ppm measured for $(NH_4)_2PdCl_6$, K_2PdCl_6 and K_2PdBr_6, respectively. A change of anion from Cl^- to Br^- in the immediate coordination sphere causes an upfield chemical shift of ∼−800 ppm due to the increased shielding caused by greater electron donation from the Br atoms to the Pd(IV) position. Changing the cations in the second coordination sphere also has an effect on the ^{105}Pd isotropic chemical shift position, as demonstrated by the comparatively smaller δ_{iso} change of ∼+10 ppm measured between K_2PdCl_6 and $(NH_4)_2PdCl_6$. These distinct shift changes of up to ∼2–3 orders of magnitude difference reflect an extreme sensitivity of the ^{105}Pd δ_{iso} values to the speciation occupying both the nearest-neighbour and next-nearest-neighbour positions upon substitution in these Pd(IV) systems.

Of great interest are the observable slopes that the data in Fig. 1(a and b) describe; the small but measurable P_Q/C_Q determined from these data are summarised in Table 1. This suite of complexes displays small P_Q values in the range of 0.47 and 0.81 MHz ($C_Q = P_Q$, assuming an η_Q of 0.0) which conflicts with the original reported crystal structures which depict octahedral Pd(IV) centres in perfect face centred cubic structures. Other octahedral inorganic compounds, containing 16-fold symmetrical centres, have been shown to exhibit a P_Q of zero due to the lack of measureable EFGs.[20,21] Hence, these data indicate a departure from perfect cubic point symmetry at the Pd positions. The very large ^{105}Pd quadrupole moment (Q) renders these positions very sensitive to the influence of structural disorder, as indicated by the MAS NMR resonances in Fig. 1(a) which exhibit a 2nd order quadrupole contribution in the centre-of-gravity shift of the central transition. This contribution is

Table 1 The ^{105}Pd and ^{39}K isotropic shift (δ_{iso}) and quadrupolar product (P_Q) NMR parameters as determined by the variable field graphical approach exploiting the centre-of-gravity/2nd order quadrupole shift B_0 dependence of the MAS NMR data, the simulation of the disorder in δ_{iso} and P_Q parameters influencing the central transition lineshape (assuming Gaussian distributions in these parameters), and the simulation of spinning sideband manifolds, for the three cubic Pd(IV) compounds

	^{105}Pd MAS NMR					^{39}K MAS NMR	
Sample	δ_{iso} (exp)[a]/(ppm)	P_Q (exp)[a]/(MHz)	δ_{iso} (sim)[b]/(ppm)	P_Q centre (sim)[b,d]/(MHz)	P_Q width (sim)[b,d]/(MHz)	δ_{iso} (exp)[a]/(ppm)	P_Q (sim)[c,d]/(MHz)
$(NH_4)_2PdCl_6$	209 ± 2	0.47 ± 0.05	211.1 ± 0.6	0.520	0.519	—	—
K_2PdCl_6	201 ± 2	0.50 ± 0.02	201.3 ± 0.3	0.520	0.519	−10.2 ± 0.5	0.007
K_2PdBr_6	−585 ± 3	0.81 ± 0.05	−584.8 ± 1.2	0.810	0.809	−16.2 ± 0.5	0.029

[a] Variable B_0 field graphical method utilising the 2nd order quadrupole shift. [b] Variable B_0 field simulation of the central transition spectrum using QUADFIT. [c] Simulation of the spinning sideband manifold using the TopSpin SOLA utility. [d] The simulation of the ^{105}Pd central transition and ^{39}K satellite transition simulation utilised an η_Q of 0 (*i.e.* $P_Q = C_Q$) and 1 (*i.e.* $P_Q = 1.15\ C_Q$), respectively.

more clearly demonstrated in Fig. 2(a–c), where the ^{105}Pd central transition lineshapes for each complex exhibits an asymmetric tail to higher field (lower frequency), indicative of a second order quadrupolar distribution due to residual structural disorder.[20–23] The quadrupolar ^{105}Pd MAS NMR lineshapes for the three disordered complexes were accurately simulated using the QUADFIT programme (see Fig. 2(a–c)), with the central values and statistical distributions governing these NMR parameters also summarised in Table 1. These values have been constrained *via* simulation at three different magnetic fields and

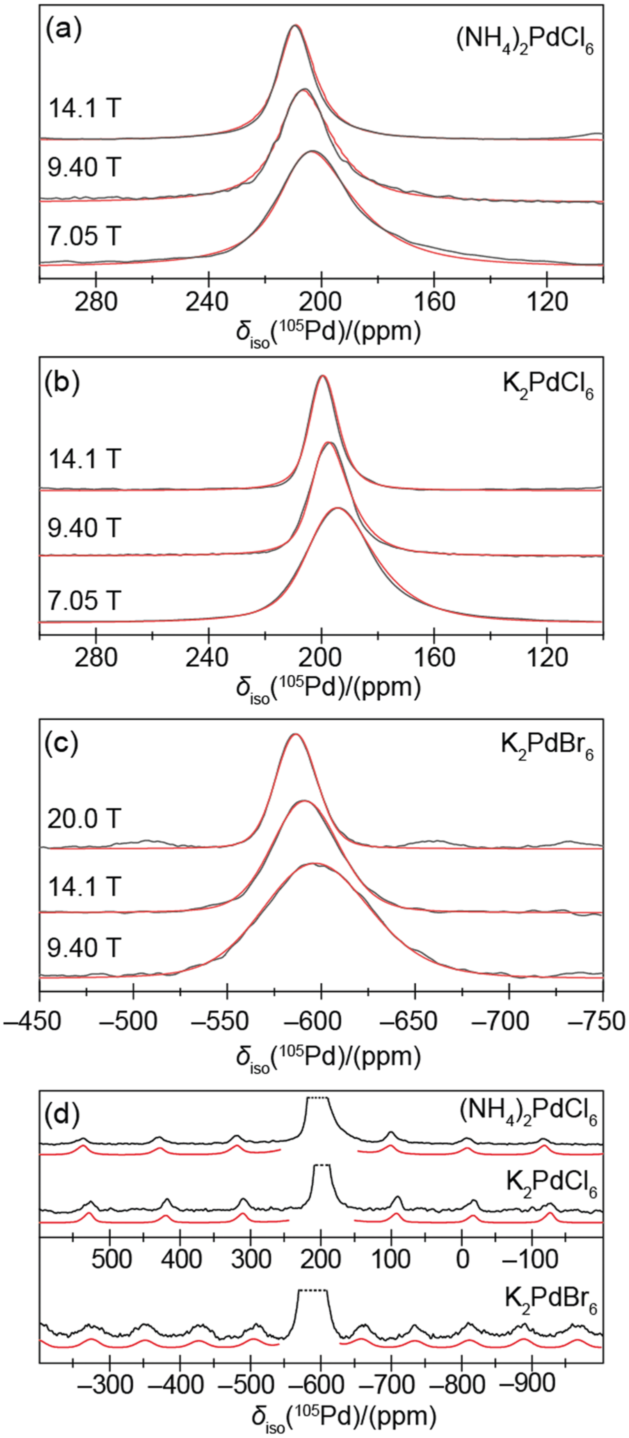

Fig. 2 The ^{105}Pd MAS NMR spectra of (a) $(NH_4)_2PdCl_{6(s)}$ at 14.1 T, 9.40 T and 7.05 T, (b) $K_2PdCl_{6(s)}$ at 14.1 T, 9.40 T and 7.05 T, and (c) $K_2PdBr_{6(s)}$ at 20.0 T, 14.1 T and 9.40 T (black); each of the disordered quadrupolar central transition lineshapes has been simulated using QUADFIT (red). (d) Expanded views of the spinning sideband manifolds of each complex at 7.05 T, 7.05 T and 20.0 T, respectively (black). The quadrupolar spinning sideband manifolds have been simulated using TopSpin (red).

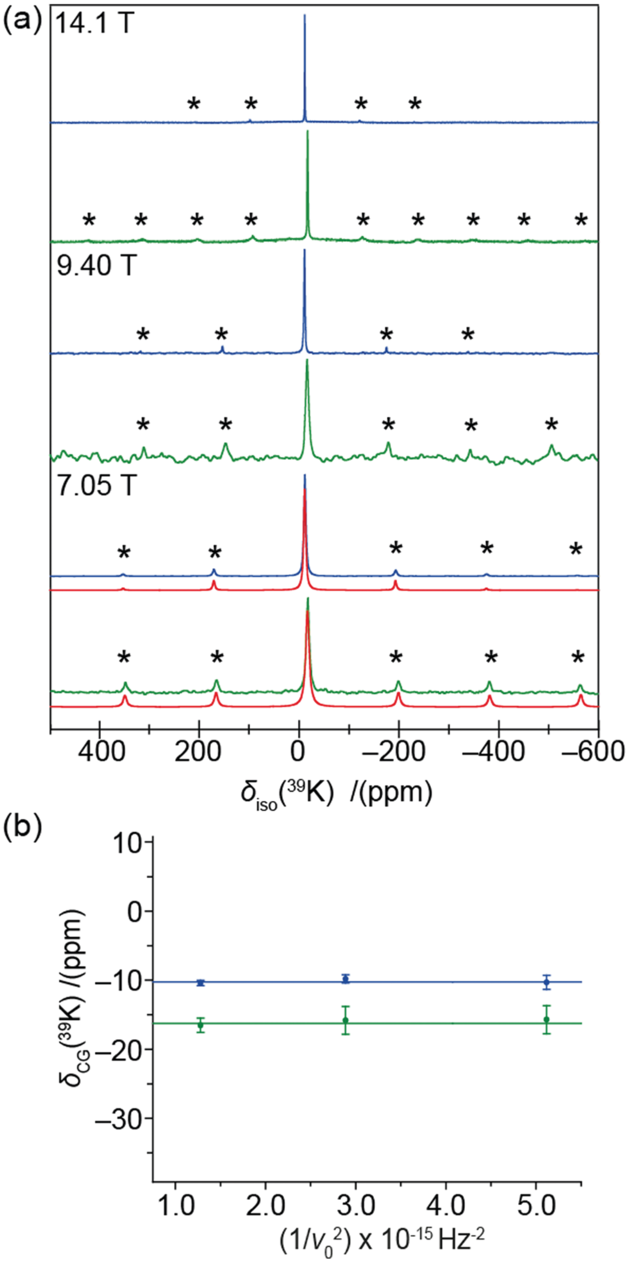

Fig. 3 (a) The ^{39}K MAS NMR data (υ_r = 3 kHz) for K_2PdCl_6 (blue) and K_2PdBr_6 (green) acquired at 14.1 T (υ_0 = 27.97 MHz), 9.40 T (υ_0 = 18.61 MHz) and 7.05 T (υ_0 = 13.98 MHz) referenced to $KCl_{(s)}$ (at δ_{iso} = 47.8 ppm). The asterisks mark the spinning sideband positions. The quadrupolar spinning sideband manifolds of both complexes at 7.05 T have been simulated (red) using Topspin. (b) The ^{39}K centre-of-gravity shifts (δ_{CG}) of K_2PdCl_6 (blue) and K_2PdBr_6 (green) plotted against the inverse square of the Larmor frequency (υ_0) at 14.1 T, 9.40 T and 7.05 T.

exhibit excellent agreement with those determined by the graphical approach shown in Fig. 1(b). The spinning sideband manifold of the ^{105}Pd MAS NMR data presented in Fig. 2(d) also supports this observation. An accurate simulation of each sideband manifold was achieved using the parameters given in Table 1. To ensure that these observations were not influenced by an impurity Pd(II) species, the complex K_2PdCl_6 was studied before and after washing with *aqua regia*; no contribution was detected as evidenced by the ^{105}Pd MAS NMR data in Supplementary Section (SI2, ESI‡).

Further evidence of this phenomenon is demonstrated by the ^{39}K and ^{35}Cl MAS NMR data presented in Fig. 3 and 4, which also indicate the existence of non-zero EFGs influencing these data. These ^{39}K MAS NMR spectra show single narrow resonances from K_2PdCl_6 and K_2PdBr_6 at $\delta_{iso} = -10.2 \pm 0.5$ ppm and $\delta_{iso} = -16.2 \pm 0.5$ ppm (calibrated against $KCl_{(s)}$ (δ_{iso} = 47.8 ppm)), respectively. The lack of a field dependent shift (Fig. 3(b)), is contradicted by the associated low intensity spinning sideband manifolds which indicate the presence of non-zero EFGs influencing the K centres which occupy the $(\frac{1}{4},\frac{1}{4},\frac{1}{4})$ positions in the $Fm\bar{3}m$ unit cell. By simulation of the spinning sideband manifolds of the 7.05 T MAS NMR data from both complexes (see Fig. 3(a)), very small P_Q values of 0.007 and 0.029 MHz can be determined for K_2PdCl_6 and K_2PdBr_6, respectively (see Table 1). In contrast to the ^{105}Pd results presented above which specifies that a 2nd order quadrupole interaction is influencing the MAS NMR data (by virtue of the very large Q), the ^{39}K MAS NMR data in Fig. 3(b) shows that there is no observable field dependent 2nd order quadrupole contribution to the observed centre-of-gravity shift position, and that the quadrupole influence upon the ^{39}K data is to 1st order only. Nevertheless, in an analogous fashion to the ^{105}Pd studies, the quadrupole contribution to the ^{39}K MAS NMR data reflects a structural disorder phenomenon in these systems. Similarly, the ^{35}Cl MAS NMR data from K_2PdCl_6 and $(NH_4)_2PdCl_6$ (Cl occupying the (0.24,0,0) positions), as observed in Fig. 4, yields narrow resonances at $\delta_{iso} = 3.6 \pm 0.8$ ppm and $\delta_{iso} = 74 \pm 2$ ppm, respectively which are also accompanied by low intensity spinning sideband manifolds. These ^{35}Cl MAS NMR data are reported against a cubic NaCl internal reference ($\delta_{iso} = -46.1$ ppm).

The non-zero EFGs detected by the NMR data imply a deviation from the perfect cubic symmetry reported by powder XRD.[19] However, X-ray pair distribution function (PDF) analyses provide descriptions of the localized structural disorder that can produce these phenomena. The real space fits of the X-ray PDF data from each Pd(IV) complex exhibits a very narrow peak at approximately 2 Å which represents a rigid and well-defined PdX_6 (X = Cl, Br) bond (see Fig. 5(a–c)). The widths of peaks from the PDF experiment represent a statistical measure of the distribution of the bond lengths, hence a very narrow peak indicates that there is no displacement of the Pd position from

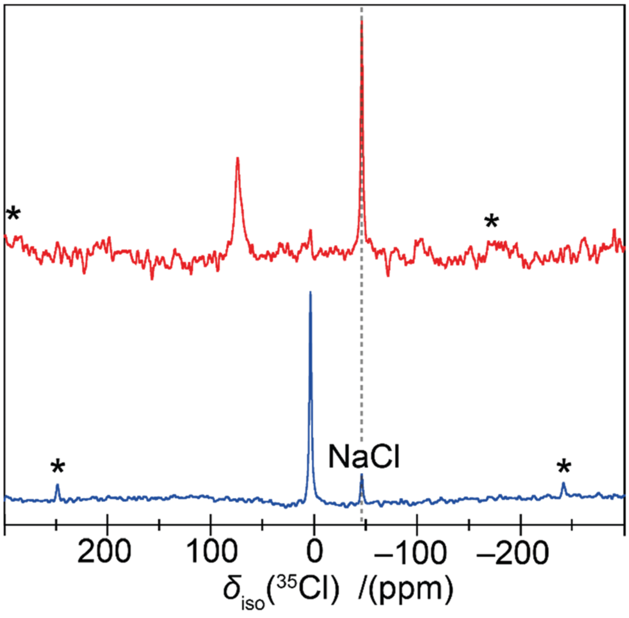

Fig. 4 The ^{35}Cl MAS NMR data (υ_r = 12 kHz) for $(NH_4)_2PdCl_6$ (red) and K_2PdCl_6 (blue) acquired at 11.7 T (υ_0 = 49.00 MHz), and internally referenced to $NaCl_{(s)}$ (at $\delta_{iso} = -46.1$ ppm). The asterisks mark the spinning sideband positions.

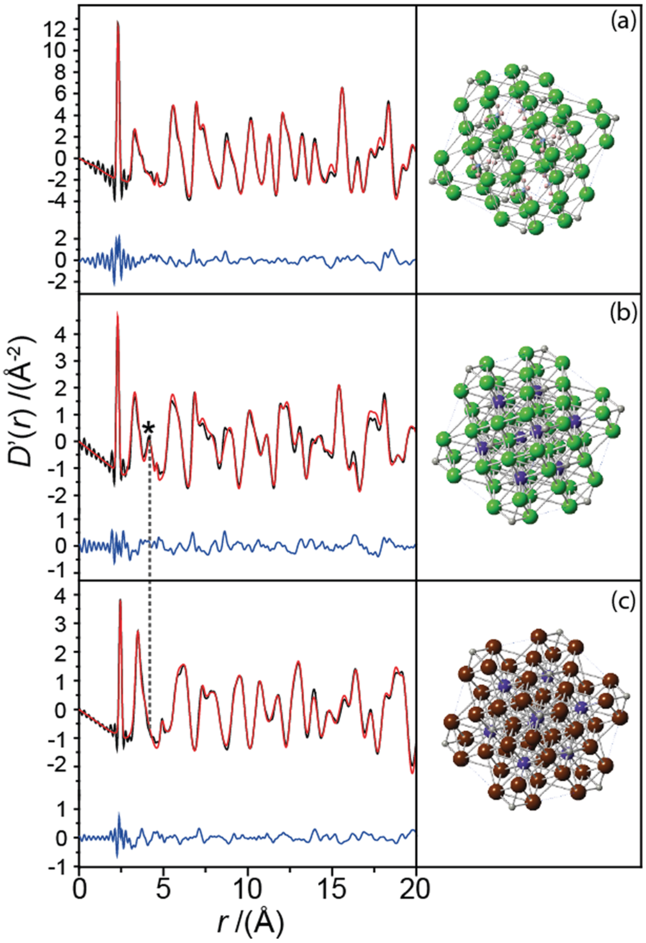

Fig. 5 Analysis of the X-ray PDF data for r = 0–20 Å with the experimental data (black), the PDF fittings (red), the offset difference curves (blue) and the refined structures for (a) $(NH_4)_2PdCl_6$, (b) K_2PdCl_6 and (c) K_2PdBr_6. The dashed black line highlights the K–Pd correlation length which is present in K_2PdCl_6, but absent in K_2PdBr_6 due to disorder.

each octahedral PdX_6 centre, as suggested from the average structure. Each octahedral hexahalopalladate unit is so well defined that the peak is at the resolution limit of the X-ray PDF measurement; this rare occurrence is responsible for the truncation artefacts observed around each 2 Å peak. Further modelling of these data also reveals that there is no measureable distortion of the Cl and Br anions from their octahedral positions. Therefore, it is highly unlikely that the deviation from cubic symmetry observed by the ^{105}Pd and ^{35}Cl MAS NMR is induced from within the octahedral PdX_6 units.

The modelling of the real space X-ray PDF date for K_2PdBr_6 (see Fig. 5(c)) requires the additional refinement of a large atomic displacement parameter for the K site exceeding what would be expected for a normal thermal parameter range. This is clear when comparing the PDF data for K_2PdCl_6 and K_2PdBr_6; the K–Pd bond lengths determined from the literature structures of both complexes are 4.2 and 4.6 Å, respectively. The accompanying peak from this length is present in the PDF data for K_2PdCl_6 (see Fig. 5(b)), but not for K_2PdBr_6. Hence, there is a negligible probability of instantaneously finding the K^+ cation precisely at the $(\frac{1}{4},\frac{1}{4},\frac{1}{4})$ position in K_2PdBr_6. This is due to the larger Br anions inducing an increased unit cell volume, thus leaving a larger residence volume for the K^+ cation to occupy. The bond valence sums (BVS) for the K^+ cations reflect this, with the K^+ position in K_2PdBr_6 showing significant underbonding (BVS of 0.845, *cf.* 1.006 for the K_2PdCl_6).[24] This deviation from cubic symmetry at the cation position explains the largest P_Q determined for K_2PdBr_6 (see Table 1), but it does not rationalise why smaller but non-zero EFGs are observed in $(NH_4)_2PdCl_6$ or K_2PdCl_6 (the former exhibits only a small peak at the ∼4 Å region because of the relative lower sensitivity of X-rays to $(NH_4)^+$ than K^+). These structures refined against the PDF data reveal no other local departures from cubic symmetry. It is therefore postulated that the hexachloride complexes are characterised by reduced degrees of disorder at their respective NH_4^+ and K^+ cation positions (compared to that observed in K_2PdBr_6), and that the extreme sensitivity of the ^{105}Pd NMR to variations in the Pd environment are enhanced by the very large ^{105}Pd quadrupole moment (Q). Such small degrees of disorder can be comprised of surface vacancies, dislocations, point defects and defect migration induced by many effects including particle size; this phenomenon has been previously observed in many MAS NMR studies of other inorganic solids including Li_2O,[25] KBr,[26] NaBr,[26] $KMnO_4$,[26] AgBr,[27] MgO[28] and NaCl.[29,30]

Table 2 Particle size distributions of the Pd metal systems determined *via* TEM statistical analysis and the experimental ^{105}Pd NMR values of the Knight shift and the full-width at half-maximum. The particle size range quoted for the bio-Pd system is a coarse estimation

		^{105}Pd	
Sample	Particle size	K_{tot} (exp)/(ppm)	FWHM (exp)/(kHz)
Pd sponge	44–149 μm	−32 050 ± 60	13 ± 1
Pd black	20–150 nm	−32 110 ± 90	16 ± 1
PVP stab. Pd	16 ± 3 nm	∼−31 100 ± 400	∼80 ± 10
Bio-Pd	2−>1000 nm	∼−31 100 ± 500	∼55 ± 15

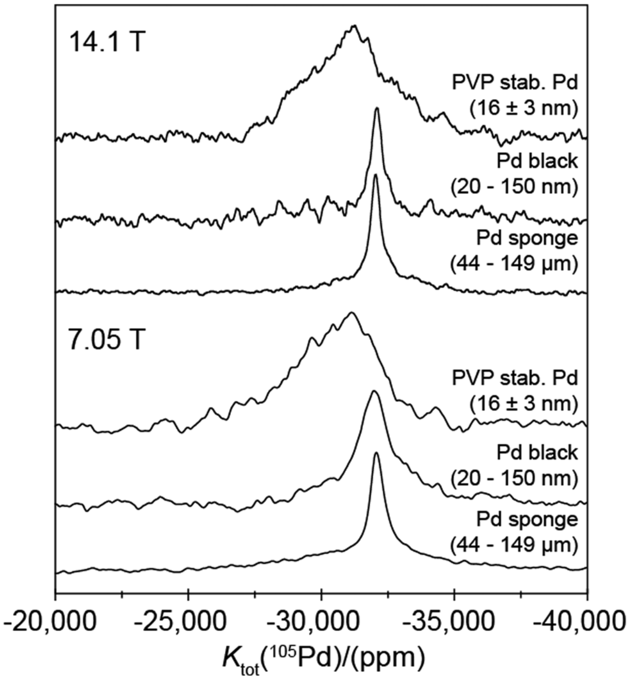

Fig. 6 The ^{105}Pd VOCS static NMR spectra PVP stabilised Pd nanoparticles (16 ± 3 nm), Pd black nanoparticles (20–150 nm) and Pd metal sponge (44–149 μm) acquired at 14.1 T, 11.7 T and 7.05 T. All data were referenced to $H_2PdCl_{6(aq)}$ (at δ_{iso} = 0.0 ppm).

This established ^{105}Pd solid state NMR methodology has also been applied to four Pd metal particle systems; Pd sponge, Pd black, poly(*N*-vinyl-2-pyrrolidone) (PVP) stabilised Pd, and bio-Pd nanoparticles. The various size distributions have been summarised in Table 2, with the nanoparticle size distributions determined *via* TEM (see Fig. 7). The ^{105}Pd static solid state NMR data of the face-centered cubic fcc Pd metal nanoparticles shown in Fig. 6 depicts conventional Knight shifted resonances, which is an interaction between the ^{105}Pd nuclei and the Pauli susceptibility of the delocalized conduction band electrons.[31] This results in an enormous shift in the resonance frequency and the total shift (K_{tot}) is often expressed as a percentage of the isotropic reference frequency. The total shift is a combination of the Knight shift (K) and a conventional shielding term (σ) as shown in eqn (5):

$$K_{tot} = K + \sigma = K_s + K_d^{orb} + K_{cp} + \sigma \qquad (5)$$

The Knight shift can be split into an s-electron contribution (K_s) and a d-electron contribution (K_d^{orb}), both of which yield positive shifts. If the hyperfine fields induce polarization of the inner shell electrons a negative shift known as the core polarization (K_{cp}) can also contribute to K and K_{tot}. The data in Fig. 6 and Table 2 clearly demonstrates that core polarization is the dominant contribution to K_{tot} for the measured Pd metal/metal nanoparticle shifts.

From Fig. 6 and Table 2, the ∼44–149 μm Pd metal (sponge) particle and the ∼20–150 nm Pd black nanoparticle systems yield similar observable resonances at K_{tot} = −32 050 ± 60 ppm and K_{tot} = −32 110 ± 90 ppm, respectively. Within experimental error these measurements both represent a K_{tot} of $-3.205 \pm 0.06\%$. This value compares favorably with a value of K_{tot} of $-3.1 \pm 0.4\%$ calculated from magnetic susceptibility measurements at 300 °C.[6] It should be noted that the small discrepancy in K_{tot} obtained from the ^{105}Pd static NMR and the magnetic susceptibility measurements is partially attributed to differences in referencing (implicit within σ, see eqn (5)), with the NMR determined K_{tot} value being measured against the proposed $H_2PdCl_{6(aq)}$ reference. In contrast to the data presented for the diamagnetic Pd(IV)-hexahalo systems above, these ^{105}Pd metal shifts for the larger ~44–149 μm Pd sponge particles and the ~20–150 nm Pd black nanoparticles are field independent (see Fig. 6 and 1(b)) indicating that no EFG can be measured (*i.e.* $P_Q = C_Q = 0$), as expected for a highly symmetrical cubic fcc structure with no observable elements of intrinsic disorder. For these cases the narrower linewidths suggest that the highly ordered bulk positions of each particle system dominates these signals in comparison to that of the lower symmetry surface positions. Further evidence for these well-formed Pd black structures is shown in the TEM images shown in Fig. 7(a and b) from which the reported particle size distribution is drawn; these images confirm the occurrence of well-defined nanoparticle structures characterising the Pd black system.

These observations contrast markedly with the ^{105}Pd static NMR data from the smaller (highly monodisperse) ~16 nm PVP-stabilised Pd nanoparticles, which exhibit a much broader, ill-defined resonance. Assuming that a cube-octahedral model describes the morphology of these PVP-stabilised nanoparticles, a Pd metal unit cell volume of 58.9 Å^3 implies that a ~16 nm particle would consist of ~150 000 Pd atoms;[32] nevertheless, the ^{105}Pd resonances measured from this highly monodisperse system do not exhibit any statistically well-defined elements of bulk character. The very high degree of monodispersity in this system is shown in the TEM images of Fig. 7(c and d) demonstrates that this observation is strictly an intra-particle phenomenon. These smaller nanoparticles have a higher ratio of surface to bulk Pd environments. Hence, despite the much greater particle size uniformity, the increased disorder and concomitant loss of translational symmetry induced by the surface and near-surface layers is reflected in these ^{105}Pd data acquired at 14.1 and 7.05 T (see Fig. 6). As exemplified by the Pd(IV)-hexahalo systems above, the very large ^{105}Pd Q value renders the NMR response to be extremely sensitive to structural perturbations causing deviation from perfect cubic fcc symmetry. The result in Fig. 6 implies that the whole ~16 nm PVP-stabilised Pd nanoparticle experiences some degree of deviation from high cubic symmetry, ranging from a large loss of symmetry at or near the surface layers, to smaller perturbations towards sub-surface and bulk regions. It is important to realise that, although the ^{105}Pd static NMR data for this system shown in Fig. 6 and 1(b) exhibits no real field dependence, this does *not* infer that on average $P_Q = C_Q = 0$ for the Pd positions within these particles. In contrast, this behavior will be underpinned by a complex relationship between the distributions of EFGs generated by the variable departure from cubic fcc symmetry depending on proximity to the particle surface, and the distributions of Knight shifts emanating from the layers comprising each particle (*e.g.* see the core–shell cubo-octahedral model in ref. 33). These assertions are supported by the absence of bulk structural components represented by a narrow resonance at $K_{\mathrm{tot}} \sim -32\,100$ ppm (see the ^{105}Pd static NMR data for the Pd black and Pd sponge in Fig. 6). The centre-of-gravity shift now occurs at an increased (more downfield) Knight shift of $K_{\mathrm{tot}} \sim -31\,100 \pm 400$ ppm demonstrating that this shift correlates with less bulk metal character (and more surface character) being realised. These results clearly demonstrate that the ^{105}Pd Knight shift is sensitive to changes in particle size and local particle symmetry.

A similar scenario is observed with the ^{105}Pd static NMR study of the highly polydisperse bio-Pd system which is reported in Fig. SI3 within the ESI.‡ In this system, the polydispersity describes a very large range of particle sizes ranging from small nanoparticles up to micron sized particles; the size range quoted above and in Table 2 represents a coarse estimate for these particles to help describe the heterogeneity in this system. This polydispersity is accompanied by a similarly large range of random particle shapes. The ^{105}Pd static NMR shows a clearly defined ordered bulk metal component to the structure within this very inhomogeneous system, as evidenced by a narrower resonance at $K_{\mathrm{tot}} \sim -32\,100$ ppm. This component is accompanied by broader downfield elements similar to those observed in the PVP-stabilised Pd system, which are attributed to smaller particles with structures that are perturbed from cubic fcc symmetry; *i.e.* those components more proximate to surface and sub-surface environments. The observation of highly variable static NMR resonance linewidths emanating from particle size effects in metal particles and nanoparticle systems has been previously described in studies on several metal species.[33,34]

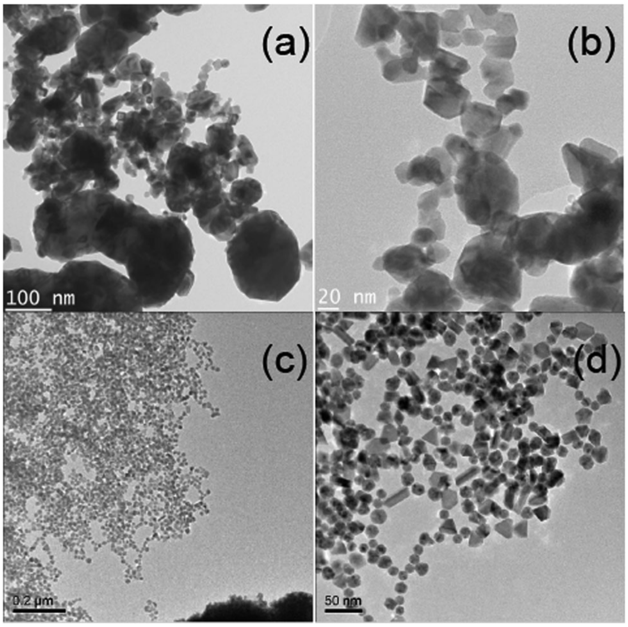

Fig. 7 The TEM images of (a), (b) ~20–150 nm Pd black nanoparticles, and (c), (d) highly monodisperse 16 ± 3 nm PVP stabilised Pd nanoparticles.

Conclusions

This study illustrates the feasibility of ^{105}Pd solid state NMR on diamagnetic and metallic systems. The large ^{105}Pd quadrupole moment gives rise to measureable EFGs that can act as a very sensitive probe of small structural distortions which are not observable by laboratory source X-ray diffractometers. X-ray PDF refinements confirm the nature of these secondary shell distortions. Future solid state ^{105}Pd NMR analyses will be aided by the proposal of standardised direct and indirect ^{105}Pd chemical shift references such as $H_2PdCl_{6(aq)}$ and KCl respectively. The ^{105}Pd Knight shift is also shown to be a sensitive probe of particle size effects in metallic systems. It has been demonstrated that the room temperature confirmation of the Knight shift of Pd metal provides an excellent basis for further ^{105}Pd studies of intermetallic (PdZn,[35] PdGa[36] and PdCu[37]) and alloyed catalysts (PtPdRh[38]) used in fuel cell, electrocatalysts and auto-catalyst technologies, and capped/stabilised nanoparticles systems used in hydrogenation reactions and fine chemical syntheses.[1–3,10–12]

Experimental

All three Pd(IV) complexes (potassium hexachloropalladate, 99%; ammonium hexachloropalladate, 99.9%; potassium hexabromopalladate, 99.9%) are commercially produced and were purchased from Alfa Aesar. Pd metal particles in the form of ~44–149 μm Pd sponge, ~20–150 nm Pd black and highly monodisperse 16 ± 3 nm PVP-stabilised Pd nanoparticles were synthesized and provided by Johnson Matthey.[11,39] A sample of highly polydisperse bio-Pd nanoparticles of average size ~2–>1000 nm (coarse approximation) was synthesized *via* the biomineralized reduction of Pd(II) to Pd(0) using *E. coli* cells and pyrolysed in vacuum.[40] The particle sizes of these Pd metal particle was determined by sampling statistics performed under transmission electron microscopy (TEM) analyses.

For the calibration of the ^{105}Pd NMR measurements the synthesis of the 0.33 M $H_2PdCl_{6(aq)}$ chemical shift reference was undertaken by the stepwise dissolution of 0.125 g of Pd metal sponge in 2 mL of concentrated (70%) HNO_3. This was followed with the addition of 4–6 mL of concentrated (36%) HCl to produce a dark red colour solution in a strongly oxidizing acid/*aqua regia* environment. The chemical equation for this reaction is proposed to be:

$$Pd_{(s)} + 4NHO_{3(aq)} + 6HCl_{(aq)} \rightarrow H_2PdCl_{6(aq)} + 4NO_{2(g)} + 4H_2O \quad (6)$$

An overall excess of *aqua regia* is required to impede the reduction of $H_2Pd(\text{IV})Cl_6$ (octahedral Pd coordination) to $H_2Pd(\text{II})Cl_4$ (square planar Pd coordination); the lower symmetry of the latter species induces a large quadrupolar broadening making it unsuitable as a ^{105}Pd chemical shift reference. To test for the possibility of Pd(II) impurities within the Alfa Aesar products, K_2PdCl_6 was added to an *aqua regia* solution to remove any potential species. This solution was allowed to stand for 60 minutes, then K_2PdCl_6 powder was then filtered from the solution, washed with distilled water and left to dry.

All room temperature ^{105}Pd MAS and static NMR measurements in this study were performed at the magnetic field (B_0) strengths of 20.0, 14.1, 11.7, 9.4 and 7.05 T using Bruker Avance III-850 (υ_0 = 39.00 MHz), Bruker Avance II+-600 (υ_0 = 27.49 MHz), Bruker Avance III-500 (υ_0 = 22.93 MHz), Bruker Avance HD-400 (υ_0 = 18.30 MHz) and Bruker Avance HD-300 (υ_0 = 13.75 MHz) spectrometers, respectively. For the hexahalo-Pd(IV) systems, both MAS and static measurements were undertaken using Bruker 7 mm HX MAS (20.0 T), Varian 9.5 mm MAS (14.1, 11.7 and 9.4 T) and Otsuka 9.5 mm MAS (7.1 T) probes, which enabled MAS frequencies of ~3–5 kHz at all fields for the acquisition of the MAS NMR data. At each B_0 field a $(\pi/4)$–τ–$(\pi/2)$–τ Hahn echo sequence was utilised to diminish ringing effects present at low frequencies, with rotor synchronized τ delays of ~330 μs and a recycle delay of 1 s being implemented throughout. For the $I = 5/2$ ^{105}Pd nucleus, non-selective (solution) $\pi/2$ pulse lengths of 30, 60, 36, 30 and 24 μs were calibrated on $H_2PdCl_{6(aq)}$ which corresponded to selective (solid) $\pi/4$ pulse lengths of 5, 10, 6, 5 and 4 μs at 20.0, 14.1, 11.7, 9.4 and 7.1 T, respectively. All ^{105}Pd chemical shifts were referenced to the proposed standard of 0.33 M $H_2PdCl_{6(aq)}$ (δ_{iso} = 0.0 ppm) and the neighbouring $KCl_{(s)}$ standard (δ_{iso} = 17 647 ppm).

The solid state NMR study of metals has several associated complications due to the conductivity of the samples. For the ^{105}Pd NMR analyses of the metal systems RF penetration (skin depth) effects must be considered, and the sample conductivity can markedly de-tune the probe. The latter aspect is alleviated by diluting each sample with NaCl to a level of 75 wt% of the salt. In addition, the build-up of eddy currents in a conductive sample will resist MAS averaging and induce heating. These details have been treated in detail elsewhere.[33] Therefore, all ^{105}Pd measurements on the metal systems were performed under static conditions. The ultra-wide linewidths exhibited by these systems necessitated the use of Variable Offset Cumulative Spectroscopy (VOCS) to achieve uniform excitation of the ^{105}Pd lineshape. This involved the acquisition of several NMR experiments over a uniformly stepped frequency range (30 kHz steps), and the summation of these individual sub-spectra to reconstitute the full spectrum.[22,41] The ^{105}Pd static NMR measurements on metallic systems were performed at 14.1, 11.7 and 7.05 T and utilized a $(\pi/2)$–τ–$(\pi/2)$ solid echo experiment to improve wide line excitation; this was stepped in 30 kHz increments across the frequency range of each total spectrum. Non-selective $\pi/2$ pulse widths of 6 μs, recycle delays of 0.01 s and τ delays of 50–150 μs were common to all experiments at each field. All data were referenced to $H_2PdCl_{6(aq)}$ (at δ_{iso} = 0.0 ppm).

The ^{39}K MAS NMR data were measured at 20.0 T (υ_0 = 39.68 MHz), 14.1 T (υ_0 = 27.97 MHz), 9.40 T (υ_0 = 18.61 MHz) and 7.05 T (υ_0 = 13.98 MHz) using Bruker 7 mm HX MAS (20.0 T), Varian 9.5 mm MAS (14.1 and 9.4 T) and Otsuka 9.5 mm MAS (7.1 T) probes, which enabled MAS frequencies of ~3–5 kHz at all fields. A single pulse experiment was used for all data acquisition, with a non-selective $\pi/2$ pulse length of 18 μs being calibrated on $KCl_{(s)}$. For the measurements at each field a selective π/6 of 3 μs, and a recycle delay of 5 s were used throughout. All ^{39}K chemical shifts are reported with respect to the primary IUPAC recommended shift reference of 0.1 M $KCl_{(aq)}$ (δ_{iso} = 0.0 ppm) *via* a secondary $KCl_{(s)}$ reference (δ_{iso} = 47.8 ppm).[5] The corresponding ^{35}Cl MAS NMR data were acquired at 11.7 T (υ_0 = 49.00 MHz) using a Bruker 4 mm HX MAS probe which delivered a MAS frequency of 12 kHz for all measurements. A single pulse experiment was used for all data acquisition, with a non-selective π/2 pulse length of 4 μs being calibrated on $NaCl_{(s)}$. The measurements utilised a selective π/4 of 1 μs, and a recycle delay of 10 s. All ^{35}Cl chemical shifts are reported with respect to the primary IUPAC recommended shift reference of 0.1 M $NaCl_{(aq)}$ (δ_{iso} = 0.0 ppm) *via* a secondary $NaCl_{(s)}$ reference (δ_{iso} = −46.1 ppm).[5]

The analysis of all solid state NMR central transition lineshapes was performed using the QUADFIT simulation programme,[42] while the simulation of the corresponding satellite transition spinning sideband manifolds in the MAS NMR data were performed using the SOLA utility within the Bruker TopSpin software package.

Total X-ray scattering experiments were performed on XPDF (beamline I15-1) at Diamond Light Source, Harwell Campus, UK. Samples were packed into 1 mm borosilicate capillaries and were illuminated with photons of energy 78.34 keV (λ = 0.1583 Å). The scattered intensity was acquired on a Perkin Elmer 1611 CP3; and calibrated against a CeO_2 standard and integrated in DAWN.[43] The integrated 1D scattering pattern was used directly for Rietveld refinement and were converted to pair distribution functions in GudrunX,[44] while the structural refinements against both the real and reciprocal space data were performed in TOPAS Academic.[45]

Conflicts of interest

There are no conflicts to declare.

Acknowledgements

JVH thanks the EPSRC for funding of project EP/P511432/1, and JVH and PTB gratefully acknowledge the EPSRC and Johnson Matthey for the CASE studentships that funded TJNH and TAP. JVH thanks the EPSRC, the University of Warwick and the Birmingham Science City Programme for partial funding of the solid state NMR infrastructure at Warwick. The latter program accessed the Birmingham Science City Advanced Materials Project 1: Creating and Characterising Next Generation Advanced Materials, which derived support from Advantage West Midlands (AWM) and the European Regional Development Fund (ERDF). JVH also thanks UK National 850 MHz Solid State NMR Facility used in this research which is funded by the EPSRC, BBSRC, the University of Warwick and the Birmingham Science City Advanced Materials Projects 1 and 2, supported by Advantage West Midlands (AWM) and the European Regional Development Fund (ERDF). Collaborative assistance from the 850 MHz Facility Manager (Dinu Iuga, University of Warwick) is acknowledged. We thank beamline I15 at Diamond Light Source (Harwell, UK) for in-house research time.

Notes and references

1 D. Jollie, *Platinum 2007*, Johnson Matthey, Royston, 2007, pp. 30–37.

2 G. G. Ertl, H. Knözinger and J. Weitkamp, *Environmental Catalysis*, Wiley-VCH, Weinheim, 1999, p. 236.

3 S. Srinivasan, *Fuel Cells: From Fundamentals to Applications*, Springer, New York, 2006, p. 691.

4 P. Raghavan, *At. Data Nucl. Data Tables*, 1989, **42**, 189–291.

5 R. K. Harris, E. D. Becker, S. M. Cabral de Menezes, R. Goodfellow and P. Granger, *Ann. Magn. Reson.*, 2002, **1**, 43–64.

6 J. A. G. Seitchik, A. C. Gossard and V. Jaccarino, *Phys. Rev.*, 1964, **136**, 1119–1125.

7 A. Narath, A. T. Fromhold and E. D. Jones, *Phys. Rev.*, 1966, **144**, 428–435.

8 P. Brill and J. Voitländer, *Ber. Bunsen-Ges.*, 1973, **77**, 1097–1103.

9 K. Matsuda, Y. Kohori and T. Kohara, *Phys. Rev. B: Condens. Matter Mater. Phys.*, 1997, **55**, 15223–15227.

10 F. A. Lewis, *Platinum Met. Rev.*, 1961, **5**, 21–25.

11 J. Cookson, *Platinum Met. Rev.*, 2012, **56**, 83–98.

12 N. Zelinsky and N. Glinka, *Ber. Dtsch. Chem. Ges.*, 1911, **44**, 2305–2311.

13 M. A. Fedotov. and V. A. Likholobov, *Russ. Chem. Bull.*, 1984, **33**, 1751–1751.

14 F. E. Beamish and J. C. van Loon, *Recent Advances in the Analytical Chemistry of Noble Metals*, Pergamon, Oxford, 1972, pp. 7–19.

15 P. P. Man, in *NMR of Quadrupolar Nuclei in Solid State Materials*, ed. R. E. Wasylishen, S. E. Ashbrook and S. Wimperis, John Wiley & Sons, Ltd, 2012, pp. 3–16.

16 M. E. Smith and E. R. H. van Eck, *Prog. Nucl. Magn. Reson. Spectrosc.*, 1999, **34**, 159–201.

17 I. L. Moudrakovski and J. A. Ripmeester, *J. Phys. Chem. B*, 2007, **111**, 491–495.

18 A. Butler and H. Eckert, *J. Am. Chem. Soc.*, 1989, **111**, 2802–2809.

19 B. Douglas and S. Ho, *Structure and Chemistry of Crystalline Solids*, Springer, 2007, pp. 127–129.

20 A. Samoson, *Chem. Phys. Lett.*, 1985, **119**, 29–32.

21 C. Jäger, *NMR Basic Principles and Progress*, Springer-Verlag, Berlin, 1994, vol. 31, p. 135.

22 J. V. Hanna, K. J. Pike, T. Charpentier, T. F. Kemp, M. E. Smith, B. E. G. Lucier, R. W. Schurko and L. S. Cahill, *Chem. – Eur. J.*, 2010, **16**, 3222–3239.

23 C. S. Griffith, V. Luca, J. V. Hanna, K. J. Pike, M. E. Smith and G. S. Thorogood, *Inorg. Chem.*, 2009, **48**, 5648–5662.

24 I. D. Brown, *The Chemical Bond in Inorganic Chemistry: The Bond Valence Model*, Oxford University Press, Oxford, New York, 2nd edn, 2016.

25 Z. H. Xie, M. E. Smith, J. H. Strange and C. Jäger, *J. Phys.: Condens. Matter*, 1995, **7**, 2479–2487.

26 J. S. Frye and G. E. Maciel, *J. Magn. Reson.*, 1982, **48**, 125–131.

27 N. Zumbulyadis and A. P. Marchetti, *Colloids Surf.*, 1990, **45**, 335–346.

28 A. V. Chadwick, I. J. F. Poplett, D. T. S. Maitland and M. E. Smith, *Chem. Mater.*, 1998, **10**, 864–870.

29 T. Yamanishi, T. Kanashiro, Y. Michihiro, Y. Kishimoto and T. Ohno, *J. Phys. Soc. Jpn.*, 1995, **64**, 643–650.

30 Y. Michihiro, T. Yamanishi, T. Kanashiro and Y. Kishimoto, *Solid State Ionics*, 1995, **79**, 40–44.

31 J. J. van der Klink and H. B. Brom, *Prog. Nucl. Magn. Reson. Spectrosc.*, 2000, **36**, 89–201.

32 R. W. G. Wyckoff, *Crystal Structures*, Interscience Publishers, New York, 2nd edn, 1963, vol. 1.

33 G. J. Rees, S. T. Orr, L. O. Barrett, J. M. Fisher, J. Houghton, G. H. Spikes, B. R. C. Theobald, D. Thompsett, M. E. Smith and J. V. Hanna, *Phys. Chem. Chem. Phys.*, 2013, **15**, 17195–17207.

34 S. Cadars, B. J. Smith, J. D. Epping, S. Acharya, N. Belman, Y. Golan and B. F. Chmelka, *Phys. Rev. Lett.*, 2009, **103**, 136802.

35 J. R. Gallagher, D. J. Childers, H. Zhao, R. E. Winans, R. J. Meyer and J. T. Miller, *Phys. Chem. Chem. Phys.*, 2015, **17**, 28144–28153.

36 M. Armbrüster, K. Kovnir, M. Behrens, D. Teschner, Y. Grin and R. Schlögl, *J. Am. Chem. Soc.*, 2010, **132**, 14745–14747.

37 H. S. Chang, K. C. Hsieh, T. Martens and A. Yang, *J. Electron. Mater.*, 2003, **32**, 1182–1187.

38 C. M. Hung, *Int. J. Hydrogen Energy*, 2012, **37**, 13815–13821.

39 A. F. S. Gouldsmith and B. Wilson, *Platinum Met. Rev.*, 1963, **7**, 136–143.

40 P. Yong, I. P. Mikheenko, K. Deplanche, D. F. Sargent and L. E. Macaskie, *Adv. Mater. Res.*, 2009, **71–73**, 729–732.

41 D. Massiot, I. Farnan, N. Gautier, D. Trumeau, A. Trokiner and J. P. Coutures, *Solid State Nucl. Magn. Reson.*, 1995, **4**, 241–248.

42 T. F. Kemp and M. E. Smith, *Solid State Nucl. Magn. Reson.*, 2009, **35**, 243–252.

43 M. Basham, J. Filik, M. T. Wharmby, P. C. Y. Chang, B. El Kassaby, M. Gerring, J. Aishima, K. Leyik, B. C. A. Pulford, I. Sikharulidze, D. Sneddon, M. Webber, S. S. Dhesi, F. Maccherozzi, O. Svensson, S. Brockhauser, G. Na'rayc and A. W. Ashtona, *J. Synchrotron Radiat.*, 2015, **22**, 853–858.

44 A. K. Soper and E. R. Barney, *J. Appl. Crystallogr.*, 2011, **44**, 714–726.

45 A. A. Coelho, P. A. Chater and A. Kern, *J. Appl. Crystallogr.*, 2015, **48**, 869–875.